

# Generating Optimally Focal and Intense Current Patterns in tES via Metaheuristic L1-L1 Search: Interior-Point vs. Simplex Algorithms

Fernando Galaz Prieto, Maryam Samavaki, and Sampsa Pursiainen

**Abstract**—This numerical simulation study investigates solving the L1-norm fitted and regularized (L1-L1) linear programming (LP) problem to find a well-localized volumetric current density in transcranial electrical stimulation (tES), where a current pattern is attached through contact electrodes attached on the skin to create a stimulus in a targeted brain region. We consider a metaheuristic optimization process where the problem parameters are selected so that the final solution found is optimal with respect to given metacriteria, e.g., the intensity and focality of the volumetric current density in the brain. We focus on the effect of the LP-algorithm on the solution. We examine interior-point and simplex algorithms, which constitute two major alternative ways to solve an LP-task; the interior-point algorithms are based on determining a feasible solution set to allow finding an optimizer via Newton’s method, while the simplex methods take steps along the edges of a polytope, subdividing the set of candidate solutions into simplicial polygons. Interior-point methods stand out among them for their complexity and predictability in terms of convergence properties at the same time. To find the current pattern, we apply five alternative optimization toolboxes: Matlab, MOSEK, Gurobi, SDPT3, and SeDuMi. We suggest that the mutual differences between these vary based on the placement of the target as well as the resolution of the two-parameter lattice. In the numerical experiments, we investigate maximizing the focality and intensity of the L1-L1 optimized stimulation current and, in the latter regard, examine its relationship to the reciprocal current pattern, maximizing the focused current density.

**Index Terms**—Transcranial Electrical Stimulation (tES), Linear Programming, L1-Norm Fitting, LP-Solvers

## I. INTRODUCTION

**T**HIS study focuses on transcranial Electrical Stimulation (tES), where currents are applied non-invasively through a montage of contact electrodes attached to the skin [1]. We aim at finding an accurate, robust, and fast linear programming algorithm to optimize a current pattern via the metaheuristic L1-norm fitted and regularized (L1-L1) method recently proposed in [2] as an approach to create a focused and intense current density inside the brain. In this approach, L1-norm fitting is applied to minimize a regularized L1-norm difference between a targeted field and a volumetric current distribution, and regularization is performed in order to control the number of nonzero currents in the current pattern, i.e., the sparsity of the current pattern.

F. Galaz Prieto, M. Samavaki, and S. Pursiainen are with Computing Sciences, Faculty of Information Technology, Tampere University, Korkeakoulunkatu 3, 33072 Tampere, Finland.

E-mail: fernando.galazprieto@tuni.fi  
Manuscript received

L1-L1 is a linear programming (LP) approach which, on top of optimizing a regularized fit between a given target and a volumetric stimulus current density resulting from the injection, performs a two-dimensional metaheuristic search to set the regularization parameter  $\alpha$  and a relative threshold  $\varepsilon$  defining the focality of the solution, respectively. The outcome will be optimal with respect to a given metacriterion, which can be, for example, the current density  $\Gamma$  at the targeted location and/or the ratio  $\Theta$  between  $\Gamma$  and the average field outside the target (nuisance field). In [2], L1-L1 is suggested to be beneficial in the optimization of  $\Theta$  between  $\Gamma$  as compared to two convex L2-norm fitting techniques: L1-regularized semidefinite programming (SDP) approach (L1L2) as well as a Tikhonov-regularized version of weighted least squares optimization proposed in [3], [4]. The general advantages of L1-fitting in those applications of inverse modelling and imaging, where spatial distributions need to be well localized, are widely known [5], [6].

Compared to the state-of-the-art in non-linear convex current pattern optimization [3], [7], [8], the L1-L1 constitutes a methodological leap forward; namely, whereas the previously published methods concentrate on maximizing the focused field locally in the vicinity of the target, given an upper bound for the nuisance field, the L1-L1 performs the fitting everywhere in the brain, optimizing both the focused and nuisance field to a degree set by the focality parameter  $\varepsilon$ . Hence, L1-L1 finds a globally optimal volumetric fit, while the state-of-the-art solutions can be considered optimal only in the local environment of the target. A global fit found by L1-L1 can be considered to enhance nuisance field suppression compared to local maximization, where the maximum obtainable focused field intensity might be limited *per se*, unless the neighborhood of the target and those areas where the nuisance field is constrained are carefully separated *a priori*.

As an LP technique, L1-L1 is straightforward to implement and achieves an appropriate computational performance. Being fundamental in solving convex optimization tasks, well-performing LP algorithms are available in various optimization packages, which typically provide interior-point and simplex methods and their hybrids for LP optimization. This study aims to evaluate and compare the performance of interior-point [9] and simplex algorithms [10] in solving the L1-L1 optimization task. These are available in the well-established and widely used commercial and open-source optimization packages, for example, in Matlab, whose LP solver `linprog` includes both kind of algorithms [9], [11] as well as in Mosek

[12] and Gurobi [13] which among other things, provide a Matlab-based alternative for `linprog` but also a variety of other means to access their LP routines. In this study, the commercial Matlab, Mosek and Gurobi are accompanied by the open-source SDP packages SDPT3 [14] and SeDuMi (Self-Dual Minimization) [15]–[17], which are applicable via the openly available CVX optimization toolbox for Matlab [18].

We perform our numerical analysis using a realistic head model, evaluating maps of the optimization results for the full brain and finding the computing times required by the different solvers. By performing the comparison our goal is to find a robust and fast algorithm that can approximate the actual optimizer well already with a comparably low lattice resolution for  $\alpha$  and  $\varepsilon$ . We pay particular attention to the maximization of  $\Gamma$  and  $\Theta$ , as well as to comparing the results obtained in the former case to those yielded by the generalized reciprocity principle [7].

The numerical results obtained show significant differences between the methods investigated in this study; the success of the metaheuristic L1-L1 search process was found to be strongly dependent on the numerical implementation and affected by the search resolution. As a central observation, the interior-point methods outperform the simplex algorithms, while the package-based discrepancies are clear. These concern, in particular, the optimization of  $\Theta$ , while each solver yields  $\Gamma$ -value close to its theoretical optimum, which is shown via the generalized reciprocity principle presented in [7]. The observed running time differences are notable considering the practical applicability of L1-L1. Without any restrictions, i.e.,  $\alpha = 0$  and  $\varepsilon = 1$ , L1L1 can be interpreted to be equivalent to optimizing the focused field alone. Based on the generalized reciprocity principle formulated in [7], the current pattern maximizing  $\Gamma$  corresponds to a bipolar montage that can be obtained by picking the most intense pair of electrodes from the backprojected solution of the optimization task.

## II. METHODS

In tES, a real  $L \times 1$  current pattern  $\mathbf{y}$  (Ampere) is injected through contact electrodes attached on the skin into subject's head where it distributes as a volume current density (Ampere per  $\text{m}^2$ ) penetrating the skull and eventually reaching the brain. The relationship between  $\mathbf{y}$  and a real  $L \times 1$  discretized volume current density  $\hat{\mathbf{x}}$  is described by the governing linear system  $\hat{\mathbf{L}}\mathbf{y} = \hat{\mathbf{x}}$ , where  $\hat{\mathbf{L}}$  is a real  $N \times L$  lead field matrix, which can be obtained as shown in [2]. We define the following two volume current density components: the focused field, where the target is non-zero, and the nuisance field, where it vanishes. The governing linear system can be split component-wise  $\hat{\mathbf{L}}_1\mathbf{y} = \hat{\mathbf{x}}_1$  and  $\hat{\mathbf{L}}_2\mathbf{y} = \mathbf{0}$ , respectively. The optimization problem to find the best match between  $\mathbf{y}$  and the target is approached in the following projected form

$$\mathbf{L}\mathbf{y} = \mathbf{x}, \quad (1)$$

where the projection of the focused field into the direction of the target constitutes the first component, that is,

$$\mathbf{L} = \begin{pmatrix} \mathbf{L}_1 \\ \mathbf{L}_2 \end{pmatrix} = \begin{pmatrix} \mathbf{P}\hat{\mathbf{L}}_1 \\ \hat{\mathbf{L}}_2 \end{pmatrix} \quad \text{and} \quad \mathbf{x} = \begin{pmatrix} \mathbf{x}_1 \\ \mathbf{0} \end{pmatrix} = \begin{pmatrix} \mathbf{P}\hat{\mathbf{x}}_1 \\ \mathbf{0} \end{pmatrix}$$

with  $\mathbf{P}$  denoting a matrix that projects a vector into the direction of  $\hat{\mathbf{x}}_1$ . The target amplitude  $\|\mathbf{x}_1\|_2$  is assumed to be  $3.85 \text{ A/m}^2$ , which is a coarse approximation for the excitation threshold of nerve fibers; for the upper limb area of the motor cortex, this value decreases from 6 to  $2.5 \text{ A/m}^2$  when the stimulus frequency decreases from 2.44 kHz (kilohertz) to 50 Hz (hertz) [19].

### A. L1-L1 optimization

The L1-L1 optimization problem [2] for tES is to minimize the following objective function:

$$\min_{\mathbf{y}} \left\{ \left\| \begin{pmatrix} \mathbf{L}_1\mathbf{y} - \mathbf{x}_1 \\ \Psi_\varepsilon[\nu^{-1}\mathbf{L}_2\mathbf{y}] \end{pmatrix} \right\|_1 + \alpha\zeta\|\mathbf{y}\|_1 \right\}, \quad (2)$$

subject to  $\mathbf{y} \preceq \gamma\mathbf{1}$ ,  $\|\mathbf{y}\|_1 \leq \mu$ , in which  $\gamma$  and  $\mu$  depict the maximum applicable current and the total dose, and  $\sum_{\ell=1}^L y_\ell = 0$ . Parameter  $\alpha$  sets the level of L1-regularization with respect to scaling  $\zeta = \|\mathbf{L}\|_1$ . Function  $\Psi_\varepsilon[\mathbf{w}]_m = \max\{|w_m|, \varepsilon\}$  for  $m = 1, 2, \dots, M$ , sets a threshold  $0 \leq \varepsilon \leq 1$  for the nuisance field with respect to scaling  $\nu = \|\mathbf{x}\|$ , meaning that entries  $(\mathbf{L}_2\mathbf{y})_m$  with absolute value below  $\varepsilon\nu$  do not actively contribute to the minimization process due to the threshold. The L1-L1 problem can be solved numerically in the following form [10] including a linear objective function

$$\min_{\mathbf{y}, \mathbf{t}^{(1)}, \mathbf{t}^{(2)}, \mathbf{t}^{(3)}} \begin{pmatrix} \mathbf{0} \\ \mathbf{1} \\ \mathbf{1} \\ \mathbf{1} \end{pmatrix}^T \begin{pmatrix} \mathbf{y} \\ \mathbf{t}^{(1)} \\ \mathbf{t}^{(2)} \\ \mathbf{t}^{(3)} \end{pmatrix} \quad \mathbf{t}^{(1)}, \mathbf{t}^{(2)}, \mathbf{t}^{(3)} \succeq \mathbf{0} \quad (3)$$

inequality constraint

$$\begin{pmatrix} \mathbf{L}_1 & -\mathbf{I} & \mathbf{0} & \mathbf{0} \\ \mathbf{L}_2 & \mathbf{0} & -\mathbf{I} & \mathbf{0} \\ -\mathbf{I} & \mathbf{0} & \mathbf{0} & -\mathbf{I} \\ -\mathbf{L}_1 & -\mathbf{I} & \mathbf{0} & \mathbf{0} \\ -\mathbf{L}_2 & \mathbf{0} & -\mathbf{I} & \mathbf{0} \\ \mathbf{I} & \mathbf{0} & \mathbf{0} & -\mathbf{I} \\ \mathbf{0} & -\mathbf{I} & \mathbf{0} & \mathbf{0} \\ \mathbf{0} & \mathbf{0} & -\mathbf{I} & \mathbf{0} \\ \mathbf{0} & \mathbf{0} & \mathbf{0} & -\mathbf{I} \\ \mathbf{0} & \mathbf{0} & \mathbf{0} & \mathbf{I} \\ \mathbf{0} & \mathbf{0} & \mathbf{0} & \mathbf{1}^T \end{pmatrix} \begin{pmatrix} \mathbf{y} \\ \mathbf{t}^{(1)} \\ \mathbf{t}^{(2)} \\ \mathbf{t}^{(3)} \end{pmatrix} \preceq \begin{pmatrix} \mathbf{x}_1 \\ \mathbf{0} \\ \mathbf{0} \\ -\mathbf{x}_1 \\ \mathbf{0} \\ \mathbf{0} \\ \mathbf{0} \\ -\varepsilon\nu\mathbf{1} \\ \mathbf{0} \\ \gamma\mathbf{1} \\ \mu \end{pmatrix}. \quad (4)$$

together with the linear equality

$$\mathbf{1}^T\mathbf{y} = 0 \quad (5)$$

To obtain the matrix and right-hand side vector of the linear system. The solution can be found in a straightforward manner using the LP optimizer functions available in optimization libraries.

### B. Optimal focality and intensity

Given a target current, we consider two meta-optimization tasks to obtain maximally focal and intense volumetric current density. The intensity is defined as the projection

$$\Gamma = \frac{\mathbf{x}_1^T \mathbf{L}_1 \mathbf{y}}{\|\mathbf{x}_1\|_2}, \quad (6)$$

of the discretized volumetric current density  $\mathbf{L}\mathbf{y}$  created by the current pattern  $\mathbf{y}$  into the direction of the target current at the target location. The focality is defined as the following current ratio:

$$\Theta = \frac{\Gamma}{\|\mathbf{L}_2\mathbf{y}\|_2/\sqrt{M}}. \quad (7)$$

The maximum intensity is obtained as

$$\Gamma_{\max} = \arg \max_{\mathbf{y}, \alpha, \varepsilon} \Gamma, \quad (8)$$

and maximum focality as

$$\Theta_{\max} = \arg \max_{\mathbf{y}, \alpha, \varepsilon} \Theta \quad \text{subject to} \quad \Gamma \geq \Gamma_0. \quad (9)$$

The latter one of these tasks can be interpreted to be meta-heuristic, as a subjectively selected metacriterion  $\Gamma \geq \Gamma_0$  is applied to maintain an appropriate intensity at the target location; this is necessary, as without a lower bound for  $\Gamma$  the intensity of the maximizer is likely to vanish.

The meta-tasks are solved approximately by discretizing the two-dimensional plane of  $\varepsilon$  and  $\alpha$  using a regular lattice with steady logarithmic increments in each direction. The actual optimization task is solved in each lattice point while the approximate solution of the meta-task is found by picking the optimum out of the candidate solutions obtained at the lattice points. The metacriterion is chosen to be  $\Gamma_0 = (3/4)\Gamma_{\max}$ .

### C. Reciprocity principle

The generalized reciprocity principle (GRP) [7] is a simple approach to obtain  $\Gamma_{\max}$  based on the reciprocity of the electromagnetic field propagation. Since it finds an exact estimate, we use it as a reference technique to evaluate the performance of the optimization algorithms.

The classical version of GRP considers the connection between the forward and reverse propagation of the electromagnetic field, which in the case of the electric field caused by brain activity, is predicted by the lead field matrix of Electroencephalography (EEG) [7], [20]. GRP states that the montage yielding  $\Gamma_{\max}$  is bipolar and can be obtained by picking the two greatest EEG electrode voltages corresponding to the desired target current in the brain. Thus, these voltages can be obtained via multiplying (projecting) the target current by the EEG lead field matrix. In this study, we define GRP analogously for the tES lead field matrix  $\mathbf{L}$  which is formulated as a mapping between electrode currents and volume current field [2]. While in the general electromagnetism, Gradient propagation is not generally reciprocal, it can be shown (Appendix A) that the bipolar montage coincides with the greatest absolute backprojected currents in the vector  $\mathbf{L}^T \mathbf{x}_1$ .

### D. LP methods

As methods to solve the LP task of Section II-A we consider interior point (IP), primal simplex (PS) and dual simplex (DS) algorithms [10], [21]. Of these, IP methods can be considered the most advanced. Those utilize Newton's method to operate in the interior of a feasible set. IP algorithms can be subdivided into primal-dual (predictor-corrector) IP methods [9], [10], [22], and barrier methods, which determine the feasible set via

a barrier function. Simplex methods are based on seeking the solution by considering the feasible set as a convex polytope and moving along its edges. This strategy is less memory-consuming than the IP iteration, but has weaker and not fully predictable convergence properties for large problem sizes compared to IP iterations whose computational complexity can be obtained explicitly [10].

### E. Primal and dual solvers

The concepts of primal and dual refer to the formulation of the LP problem; noting that by presenting the entries of  $\mathbf{y}$  as differences of non-negative variables ( $y_i = s_i - p_i$ ,  $s_i, p_i \geq 0$ ) and presenting the equality constraint (5) via two inequalities (condition  $a = 0$  is satisfied  $a \leq 0$  and  $-a \leq 0$ ) the task (3)–(5) can be brought back to the following standard primal formulation:

$$\max_{\mathbf{z}} \mathbf{c}^T \mathbf{z} \quad \text{subject to} \quad \mathbf{A}\mathbf{z} \leq \mathbf{b}, \quad \mathbf{z} \geq 0, \quad (10)$$

whose dual is given by

$$\min_{\hat{\mathbf{z}}} \mathbf{b}^T \hat{\mathbf{z}} \quad \text{subject to} \quad \mathbf{A}^T \hat{\mathbf{z}} \geq \mathbf{c}, \quad \hat{\mathbf{z}} \geq 0. \quad (11)$$

### F. Solver packages

The IP algorithms applied this study include Gurobi's parallel barrier method and the primal-dual routine of Matlab, Mosek, SDPT3, and SeDuMi. The simplex methods applied include Mosek's PS and DS, Gurobi's PS and DS and Matlab's DS algorithm. Matlab's Optimization toolbox has two IP solvers of which we apply the interior-point legacy (IPL) whose origin is in the Linear-programming Interior Point SOLvers (LIPSOL) package [11]. The solvers, their types and abbreviations are described in Table I.

### G. Computing platform

The numerical simulations of this study were performed using Dell 5820 workstation with a 10-core Intel Core i9-10900X processor and 256GB RAM. The L1-L1 solver was implemented using the Matlab-based Zeffiro Interface (ZI) toolbox<sup>1</sup> [23]–[25] which builds a high-resolution finite element (FE) mesh and generates a tES lead field matrix [2] for a given surface-based head segmentation incorporating the Complete Electrode Model (CEM) [26], [27]. The solver packages (Section II-F) were accessed by ZI via their Matlab (R2020b) interfaces (I).

### H. Domain

A realistic 1 mm FE mesh was applied as the domain of the numerical simulations. This mesh was generated based on an open T1-weighted Magnetic Resonance Imaging (MRI) dataset<sup>2</sup>. The data were first segmented using FreeSurfer Software Suite<sup>3</sup> which finds the complex surface boundaries between different tissue compartments, including the skin,

<sup>1</sup>[https://github.com/sampsapursiainen/zeffiro\\_interface](https://github.com/sampsapursiainen/zeffiro_interface)

<sup>2</sup><https://brain-development.org/ixi-dataset/>

<sup>3</sup><https://surfer.nmr.mgh.harvard.edu/>

TABLE I: Detailed descriptions LP solvers applied in this study. All solvers were interfaced with Matlab’s version R2020b and called by L1-L1 optimizer of the Zeffiro Interface (ZI) toolbox [23]. As computing hardware, we used Dell 5820 workstation with a 10-core Intel Core i9-10900X processor and 256GB RAM.

Abbreviation	Solver	Interface	Method name	Method type
Gurobi IP	Gurobi Optimizer 9.5.2	Gurobi toolbox	interior-point	parallel barrier
Gurobi PS	Gurobi Optimizer 9.5.2	Gurobi toolbox	simplex	primal
Gurobi DS	Gurobi Optimizer 9.5.2	Gurobi toolbox	simplex	dual
Matlab IPL	R2020b linprog / LIPSOL	Optimization toolbox	interior-point legacy	primal-dual
Matlab PS	R2020b linprog	Optimization toolbox	simplex	primal
Matlab DS	R2020b linprog	Optimization toolbox	simplex	dual
Mosek IP	Mosek 9.1.0	Mosek toolbox	interior-point	primal-dual
Mosek PS	Mosek 9.1.0	Mosek toolbox	simplex	primal
Mosek DS	Mosek 9.1.0	Mosek toolbox	simplex	dual
SDPT3 IP	SDPT3 4.0	CVX 2.2	interior-point	primal-dual
SeDuMi IP	SeDuMi 1.1	CVX 2.2	interior-point	primal-dual

skull, cerebrospinal fluid (CSF), gray and white matter and subcortical structures such as brain stem, thalamus, amygdala, and ventricles [28]. The conductivity values of the different tissue layers were set according to [29].

I. Current field and targets

To solve the inverse problem, we discretized the current field using 563 spatial degrees of freedom which were evenly spread over the brain, i.e., those compartments that are enclosed by the skull and CSF compartments in the model. Each target position contained three divergence-free Cartesian field components. To maintain the total dose, i.e., the total current flowing through all the electrodes within acceptable limits, we choose  $\mu = 4$  mA which is a typical value in experimental studies along with 2 mA. The limit  $\gamma$  for the maximum injectable current is set to be half of the maximum dose, i.e.,  $\gamma = \mu/2$ .

J. Two-stage lattice search

The meta-optimization tasks for  $\Theta_{max}$  and  $\Gamma_{max}$  were calculated using a two-dimensional lattice covering the ranges from -160 to 0 decibels (dB) for  $\epsilon$  and from -100 to -20 for  $\alpha$ . Two different lattice resolutions  $15 \times 15$  and  $40 \times 40$  were used to examine the sensitivity of the algorithms to parameter variation. To obtain the best the optimization outcome, the meta-optimization process was run in two stages; in the first one the full set of 128 electrodes were included in the optimization process, and in the second one, the montage of the most intense 20 electrodes was fixed and the optimization process was performed in this subset. The final result was thresholded in order to count the number of non-zero (NNZ) currents in the pattern: the values smaller than 0.1 % the maximum current in the pattern were set to zero.

K. Solver packages

III. RESULTS

Figure 2 shows the results obtained in the first and second optimization stage for the somatosensory, auditory and occipital target, demonstrating the performance differences between the optimization methods. As expected, DS and PS tend to be faster but overall less accurate compared to the IP algorithms, which is clearly visible in the results obtained for  $\Theta_{max}$ ,

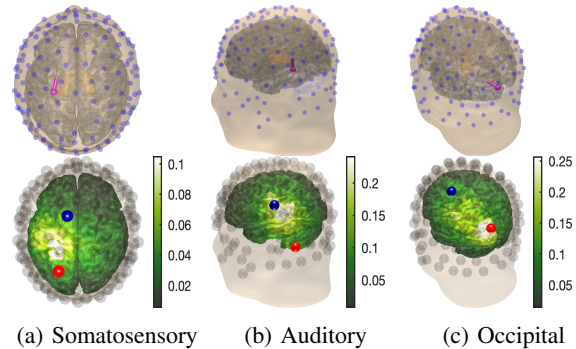


Fig. 1: **Top:** The head model and the distribution of the 128 electrode positions (blue) together with the placement of three targets (purple): somatosensory, auditory and occipital. **Bottom:** Reciprocal bi-polar current patterns maximizing  $\Gamma$  at the corresponding locations. The total dose of the current pattern is 4 mA and the volumetric current density is given in Amperes per square meter ( $A/m^2$ ).

whereas the differences observed in the estimates of  $\Gamma_{max}$  are minor, especially when the denser lattice is used. Somewhat surprisingly, Matlab IPL, the legacy routine of the LIPSOL package, is the winner method considering the amplitudes of both focality  $\Theta_{max}$  and intensity  $\Gamma_{max}$  after two optimization runs. For the somatosensory target, each algorithm finds the bipolar montage which maximizes the intensity  $\Gamma_{max}$ , while this is not the case for the other two targets. Solutions with more than two active electrodes are found by Mosek IP, SeDuMi IP, SDPT3 IP, Mosek PS, and Gurobi DS with the denser  $40 \times 40$  lattice and Mosek IP, SeDuMi IP, SDPT3 IP, Gurobi DS, Gurobi PS, Matlab DS, and Mosek DS with the coarser  $15 \times 15$  lattice.

Whereas the best mathematical performance is obtained with Matlab IPL, the open solver of the LIPSOL package, the commercial solvers are fast. Looking at the computing times in the first and second stages (Figures 2), the first stage takes up to 10000 seconds vs the second stage takes up to 1000 seconds for the denser lattice. It is obvious that the second stage must be faster to be evaluate, since it involves a limited montage and, thereby, a reduced lead field size which is roughly 15 % of the original. MOSEK IP, DS and PS turned out to be by far superior regarding the total computing time, MOSEK DS

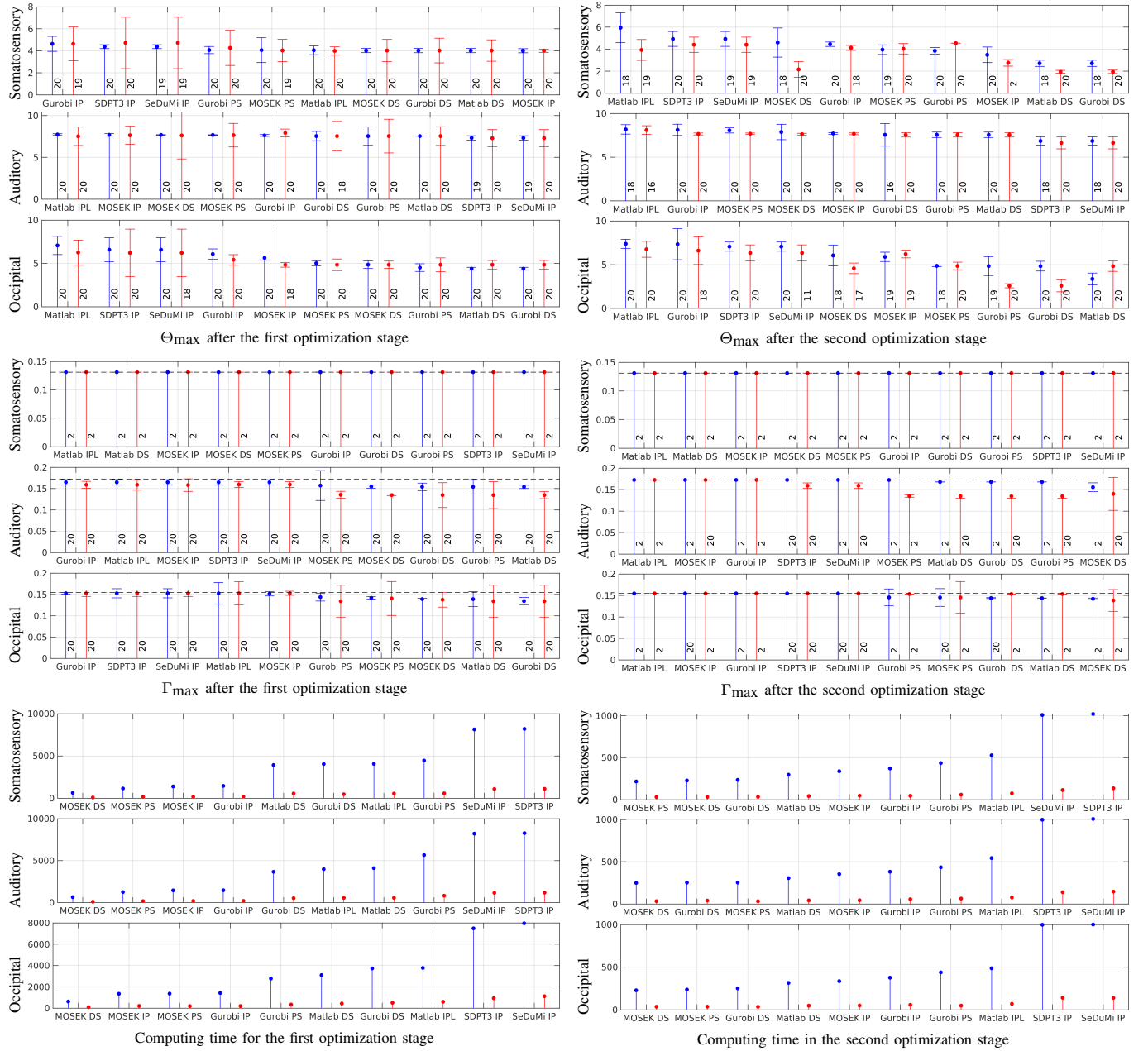


Fig. 2: **Left:** A stem plot of the first-stage optimization results obtained for the somatosensory, auditory and occipital target. The blue and bar show the results for the denser  $40 \times 40$  and coarser  $10 \times 10$  lattice, respectively. The results obtained with different optimization algorithms have been sorted into a descending order for  $\Theta_{\max}$  and  $\Gamma_{\max}$  and in an ascending order for the computing time from left to right based on the former one of these two cases. The computing time is presented as the total time required by the solvers counting together the time required by each processor core. The number of non-zero currents in the optimized pattern is shown next to the stem. The reference value obtained for  $\Gamma_{\max}$  using the reciprocity principle is shown as a dashed horizontal line. Approximating the accuracy of the lattice search, the whiskers for  $\Theta_{\max}$  and  $\Gamma_{\max}$  show a second order Taylor’s polynomial based estimate for the maximum deviation of the result within  $1/2$  lattice units distance from the optimizer. The denser lattice can be observed to have a reduced deviation compared to the coarser one, demonstrating an improved reliability of the results. **Right:** The second stage results can be observed to, improve the results compared to the first one which is obvious, e.g, based the active electrode counts obtained for  $\Gamma_{\max}$  (the bipolar exact solution has two active electrodes). The computing times are only a fraction of those required in the first stage as the limited current pattern allows a reduced representation of the lead field.

being the fastest of these three. The computing time of Gurobi IP was close to that of MOSEK IP, while Gurobi DS and PS

a well as Matlab IPL and DS required approximately three times that. The slowest performing SDPT3 and SeDuMi took

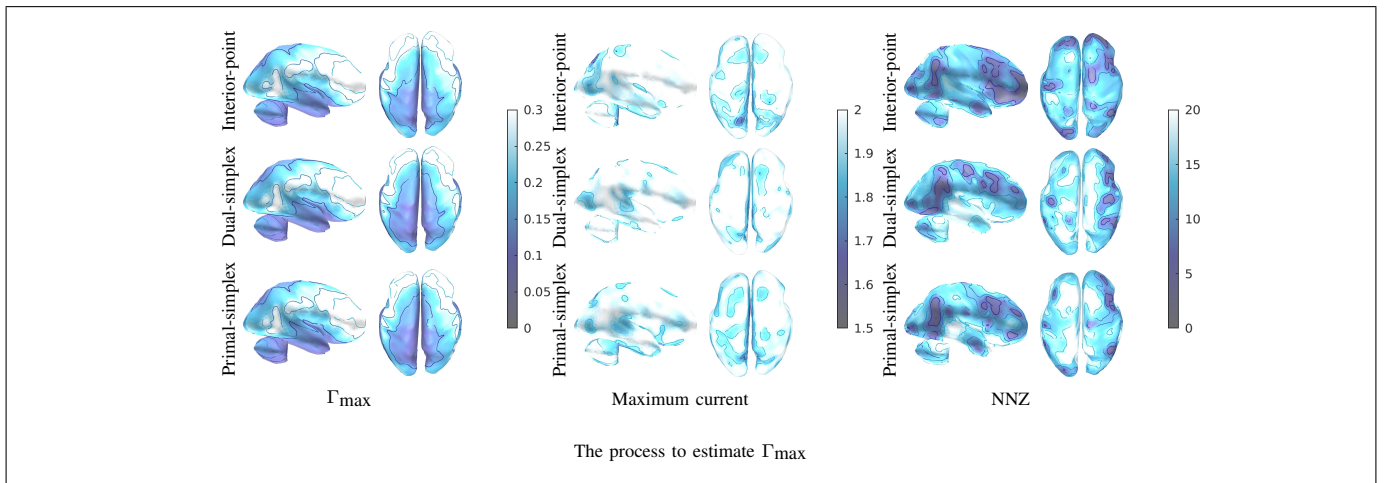
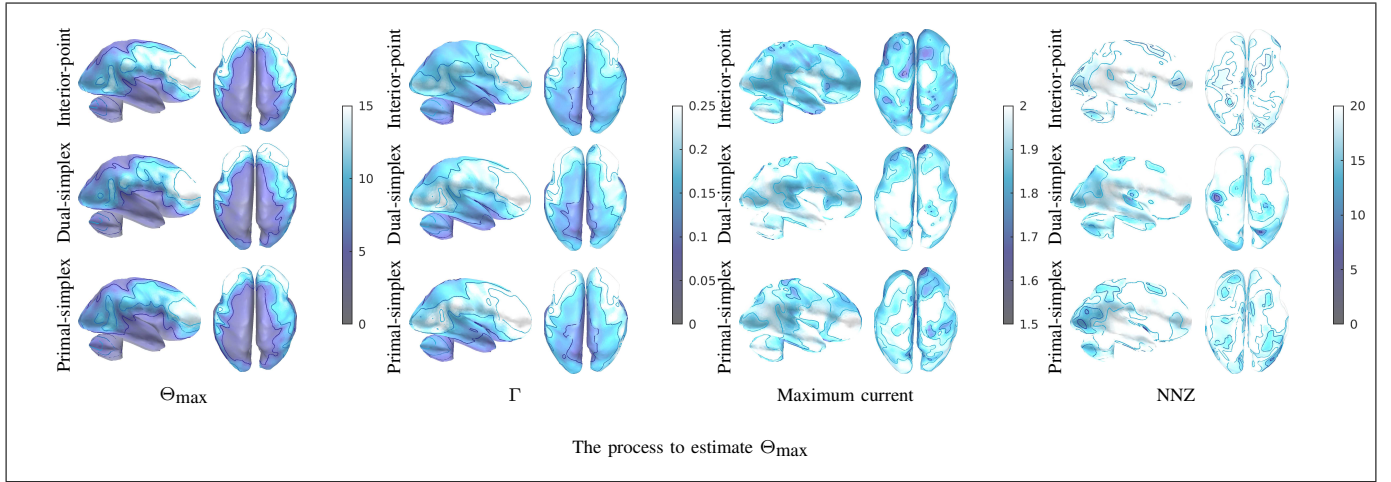


Fig. 3: **Top:** Maps of the maximum focality  $\Theta_{\max}$  and the values of intensity  $\Gamma$ , the maximum current and NNZ corresponding to the maximizer for coarser  $15 \times 15$  lattice and the interior-point (IP), dual-simplex (DS) and primal-simplex (PS) algorithm of the MOSEK package. Each map includes contours for 20, 40 and 75 % of the maximum entry. While the maps obtained with different algorithms are topographically similar, IP can be observed to enhance  $\Theta_{\max}$ , especially, in the areas, where the solutions are likely to be focal. In these areas, DS and PS yield a greater intensity which comes with the cost of suppressed focality. **Bottom:** Maps of the maximum intensity  $\Gamma_{\max}$ . The mutual differences between the maps are minor, both topographically and amplitude-wise. Of  $\Theta_{\max}$  and  $\Gamma_{\max}$ , the former one corresponds to a greater NNZ and a smaller maximum current.

as much as six times the run time of MOSEK IP.

For their fast performance, we applied MOSEK IP, DS and PS together with the  $15 \times 15$  search lattice to evaluate maps of  $\Theta_{\max}$  and  $\Gamma_{\max}$  by solving the optimization task for each spatial and directional degree of freedom in the discretized source distribution (Figure 3). These maps were observed to be mutually similar between the three solvers. In the case of the focality  $\Theta_{\max}$  (first row), the IP optimizer achieves enhanced amplitudes compared to DS and PS in the area, where finding a focal stimulus can be considered feasible. In these areas, DS and PS yield a greater intensity which comes with the cost of suppressed focality and is less interesting in the process to find  $\Theta_{\max}$  as it does not primarily aim at maximizing the intensity but the focality instead. The maps obtained for  $\Gamma_{\max}$  (second row) have minor differences both

topographically and amplitude-wise. Of  $\Theta_{\max}$  and  $\Gamma_{\max}$ , the former one corresponds to a greater NNZ and a smaller maximum current. A smaller number of NNZ in finding  $\Gamma_{\max}$  is expected, since the optimizers often find the bipolar pattern. Hence, the overall current pattern has a greater coverage but a smaller maximal intensity in the case  $\Theta_{\max}$  compared to the case of  $\Gamma_{\max}$ .

Figure 4 shows the first-stage lattice search of the meta-optimization processes:  $\Theta_{\max}$  (purple star) is found using as a metacriterion the threshold condition corresponding to 75% of the maximum amplitude obtainable with the bipolar two-channel montage, and  $\Gamma_{\max}$  is the global maximizer of  $\Gamma$  (yellow star). The search results are shown for each optimization algorithm for two different lattice resolutions  $15 \times 15$  and  $40 \times 40$ . In the denser lattice, a thin vertical line maximizing

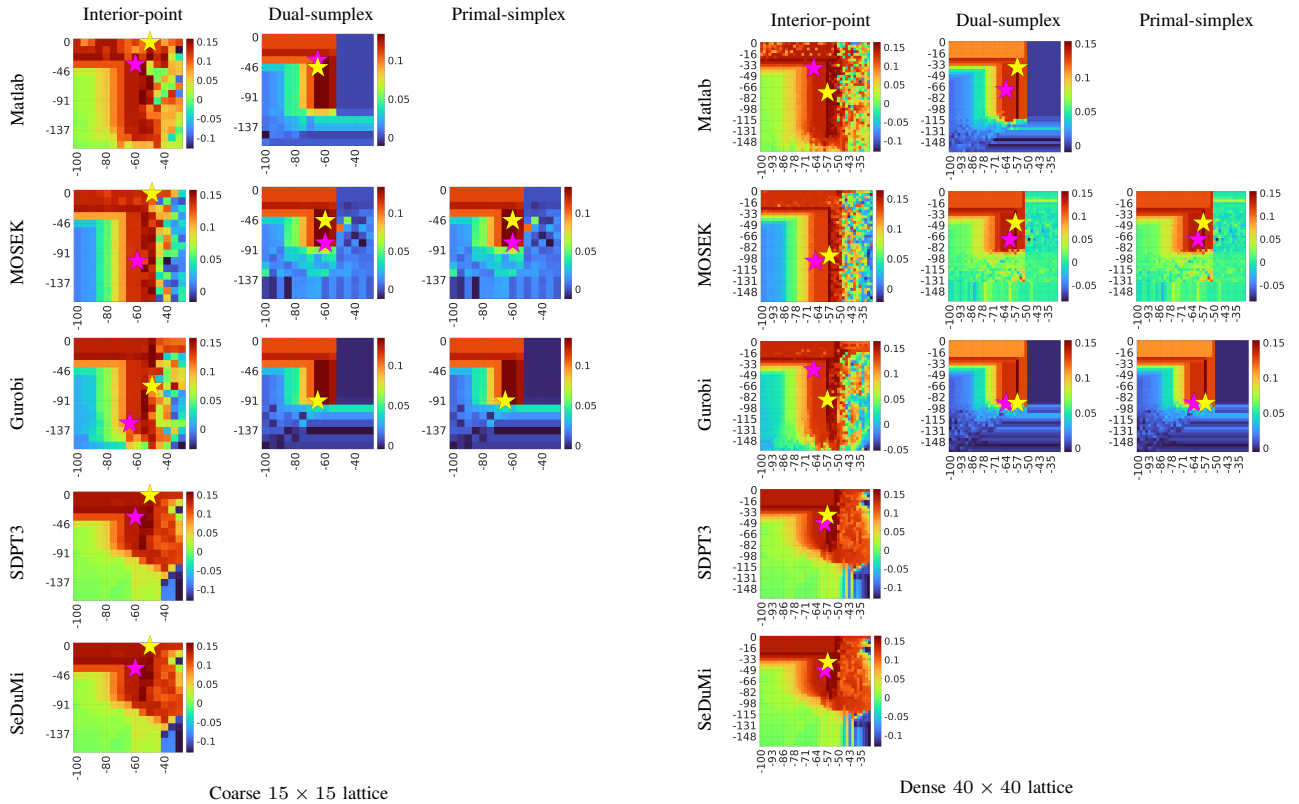


Fig. 4: **Left:** Charts showing value of  $\Gamma$  in the  $15 \times 15$  coarser  $\alpha\epsilon$ -lattice of the two-stage meta-optimization process for different optimization processes. The yellow star shows the maximizer of the intensity  $\Gamma_{\max}$  and purple one that of the focality  $\Theta_{\max}$ . The maximizers are rather generally found with  $\epsilon$ -values (threshold levels) smaller than  $-30$  dB, reflecting the mutual scale difference between the reference amplitude of  $x_1$  and the volumetric current intensities that can be generated within the given limits for the maximum dose. The regularization parameter  $\alpha$  can be observed to have a sweet spot between  $-60$  and  $-50$  dB, where the intensity obtains its maximum. The maximum focality is found with a slightly smaller  $\alpha$  compared to the intensity. Significant mutual differences can be observed between how the different optimization methods localize the sweet spot; in particular, the IP algorithms tend to find a smoother area with an elevated  $\Gamma$  than the simplex methods. **Right:** Charts showing the denser  $40 \times 40$   $\alpha\epsilon$ -lattice for  $\Gamma$ . Compared to the coarser sweet spot between  $-60$  and  $-50$  dB can be observed to be sharper and to have an enhanced amplitude, in particular, in the case of the DS and PS algorithm, suggesting that they might be less robust than IP with respect to the selection of  $\alpha$  and  $\epsilon$  parameter.

current amplitude is well visible. This sweet spot appears in the regularization parameter range from  $-60$  to  $-50$  dB (horizontal axis) and the nuisance field threshold range below  $-30$  dB. Emphasizing the importance of a sufficient search resolution, the denser lattice contains some details that are absent in the coarser lattice which affect the optimization process. For the IP algorithms, the lattice structure is overall smoother and the differences between the two resolutions are less drastic than for DS and PS. Hence, it seems that DS and PS methods are less robust regarding the variation of the search parameters as compared to the IP techniques, partially explaining the mutual performance differences between IP, DS and PS observed in the numerical experiments of this study.

The denser lattice not only increases the optimization accuracy but also the numerical stability of the results; the denser lattice deviates less in the vicinity of the optimum than the coarser one which can be observed in Figure 2 based on the whiskers showing second order Taylor’s polynomial estimates for the maximal deviation within a  $1/2$  lattice size distance

from the optimizer position.

#### IV. DISCUSSION

In this study, we compared the performances of several IP [9], DS and PS algorithms [10] to solve the recently introduced L1-L1 (L1 fitted and regularized) optimization task of tES [1]. These techniques are currently the predominating ones in solving Linear Programming (LP) problems, and therefore they are available in most open and commercial optimization toolboxes. The comparison was motivated by our earlier results [2] which suggest that L1-L1 provides a theoretically attractive approach to obtain a focal stimulus with a focal current pattern and that it performs appropriately compared to complex L2-fitting and regularized least squares techniques [2]. In particular, the optimization process itself is completely parameter free and does not necessitate any prior knowledge about where and how much the nuisance field needs to be suppressed, which is the case in the earlier LP formulations of the tES current optimization problem [3], [7], [8]. In L1-L1,

the nuisance field is settled optimally by a meta-optimization process that is performed in a two-dimensional lattice.

We examined solvers of the commercial Matlab, Mosek [12] and Gurobi [13] toolboxes as well as SDPT3 [14], SeDuMi (Self-Dual Minimization) [15]–[17] which are openly available and accessible through the open CVX toolbox for Matlab [18]. Even though commercial, Matlab IPL, i.e., Matlab’s legacy IP solver, can also be regarded as an open, since it originates from the open LIPSOL [11] toolbox. It was selected to this study, since Matlab’s main IP algorithm was observed to stall in the middle of a two-stage meta-optimization process and not return an appropriate result at all.

As a reference technique in the comparison, we used the generalized reciprocity principle (GRP) [7], which states that, given the target, the current pattern corresponding to the maximum intensity can be obtained by picking the two electrodes with the largest absolute backprojected currents. The validity of GRP was shown for the present lead field matrix  $\mathbf{L}$  (Appendix A), since the reciprocity of propagation concerns an electromagnetic field itself, measured for instance in EEG, but not necessarily the gradient of the field evaluated by  $\mathbf{L}$  which projects the current flux through the boundary electrodes to a volumetric current density.

In the numerical experiments, we observed significant mutual differences between the solvers. These differences concern mainly the greatest obtainable focality amplitudes and the number of active electrodes, whereas rather similar intensities and topography maps could be obtained regardless of the method. A somewhat surprising finding was that Matlab IPL demonstrated superior mathematical performance in the mutual comparison between the different solvers; it was the winner after two optimization runs considering both  $\Theta_{\max}$  and  $\Gamma_{\max}$  for each target location. The commercial solvers were observed to be fast compared to the other methods, especially MOSEK IP, DS, and PS, which were the fastest of their kind in this study. While the best performing solvers show that the L1-L1 method is suitable for maximizing both focality and intensity, a few of them did not find the bipolar current pattern that maximizes  $\Gamma_{\max}$ . Notably, SDTP3 did not find a bipolar pattern at all, verifying our earlier hypothesis [2] that the performance of L1-L1 might be highly solver-based. Part of the discrepancies between the optimization methods can obviously be explained by a different sensitivity with respect to parameter variation or the resolution of the meta-optimization lattice.

The IP, DS and PS methods were natural choices for this study, since they are available in well-known optimization packages. As DS and PS require fewer machine resources than the IP methods and provide an appropriate estimate  $\Gamma_{\max}$ , they might be beneficial in some applications, where the hardware performance is limited, for example in a potential FPGA implementation of the L1-L1 optimizer [30], [31]. Otherwise, IP algorithms seem preferable due to their better mathematical performance for the L1-L1 task. Alternative solver algorithms might include Alternating Direction Method of Multipliers (ADMM) [32] which is increasingly applied to LP problems. ADMM was not included in this investigation, as achieving an appropriate convergence with ADMM seemed more difficult,

e.g., due to its dependence on a step-length parameter.

As for the future work, we currently plan to use L1-L1 in applications. One interesting application would be deep brain stimulation (DBS), where an advanced optimization technique is needed to target the subcortical nuclei of the brain. See, for example, a recent study [33], where an IP algorithm has been applied.

#### ACKNOWLEDGMENT

FGP, MS, and SP were supported by the Academy of Finland Center of Excellence in Inverse Modelling and Imaging 2018–2025, DAAD project (334465) and by the ERA PerMed project PerEpi (344712).

#### APPENDIX

GRP can be formulated for a restricted system  $\mathbf{L}\mathbf{R}_K\mathbf{y}_K = \mathbf{x}$ , where  $\mathbf{R}_K$  denotes a real  $N \times K$  ( $K \leq N$ ) restriction matrix, whose nonzero entries  $r_{i_j,j} = 1$  corresponds to an ordered subset of electrodes  $\mathcal{S} = \{i_j : j = 1, 2, \dots, K\}$ , with  $|(\mathbf{L}_1^T \mathbf{x}_1)_{i_1}| \geq |(\mathbf{L}_1^T \mathbf{x}_1)_{i_2}| \geq \dots \geq |(\mathbf{L}_1^T \mathbf{x}_1)_{i_K}|$ . GRP follows by writing the intensity as  $\Gamma = \sigma_K \mathbf{y}_K^T \mathbf{s}_K$  with  $\sigma_K = \|\mathbf{R}\mathbf{L}_1^T \mathbf{x}_1\|_1 / \|\mathbf{x}_1\|_2$  and  $\mathbf{s}_K = \mathbf{R}\mathbf{L}_1^T \mathbf{x}_1 / \|\mathbf{R}\mathbf{L}_1^T \mathbf{x}_1\|_1$  which shows that  $\Gamma$  can be interpreted as a projection of  $\mathbf{y}_K$  on  $\sigma_K \mathbf{s}_K$ .

Thus, the maximum of  $\Gamma$  is obtained, when  $\mathbf{y}_K$  is parallel to  $\mathbf{s}_K$ . Since the maximizer also needs to match the maximum applicable dose  $\mu$ , as otherwise it can be upscaled, it follows that  $\mathbf{y}_K = \mu \mathbf{s}_K$ . The corresponding maximum intensity is  $\Gamma = \mu \sigma_K \|\mathbf{s}_K\|_2^2$ . The optimal montage is the maximizer of

$$\max_K \mu \sigma_K \|\mathbf{s}_K\|_2^2, \quad (12)$$

where by definition  $\|\mathbf{s}_K\|_1 = 1$  and the entries of  $\mathbf{s}_K$  are ordered in a descending order with respect to their absolute value. Assuming that these entries are given by  $\sum_{j=1}^K \lambda_j$  with  $\lambda_1 \geq \lambda_2 \geq \dots \geq \lambda_K \geq 0$  it holds that  $\|\sum_{j=1}^K \lambda_{i_j}^2\|$

$$\begin{aligned} \|\mathbf{s}_K\|_2^2 - \|\mathbf{s}_{K-1}\|_2^2 &= \frac{\lambda_K}{1 - \lambda_K} \left( \lambda_K^2 - \lambda_K + 2 \sum_{j=1}^{K-1} \lambda_{i_j}^2 \right) \\ &\geq \frac{\lambda_K}{1 - \lambda_K} \left( K \lambda_K^2 - \lambda_K + \sum_{j=1}^{K-1} \lambda_{i_j}^2 \right) \end{aligned} \quad (13)$$

Here the equality follows from a straightforward substitution and the inequality is obtained as  $(K - 1)\lambda_K^2 \leq \sum_{j=1}^{K-1} \lambda_{i_j}^2$ . Following from the discriminant together with the Arithmetic Mean – Quadratic Mean inequality

$$\frac{1}{K-1} \sum_{j=1}^{K-1} \lambda_{i_j}^2 \geq \left( \frac{1}{1-K} \sum_{j=1}^{K-1} \lambda_{i_j} \right)^2, \quad (14)$$

the second factor in (13) does not have roots if

$$K \sum_{j=1}^{K-1} \lambda_{i_j}^2 \geq \left( \sum_{j=1}^{K-1} \lambda_{i_j} \right)^2 \geq \frac{1}{4}. \quad (15)$$

That is, if  $\sum_{j=1}^{K-1} \lambda_{i_j} \geq \frac{1}{2}$ . This assumption is valid, since a montage can have minimally two active channels, none of



which can contain more than half of the total dose, since the sum of currents for any montage is assumed to be zero. Hence, it follows that  $\|s_K\|_2^2 - \|s_{K-1}\|_2^2 \geq 0$  for any montage and, recursively, that the maximum of  $\Gamma$  is obtained with the bipolar pattern that corresponds to the first two entries  $i_1$  and  $i_2$  in the set  $\mathcal{S}$ .

## REFERENCES

- [1] C. S. Herrmann, S. Rach, T. Neuling, and D. Strüber, “Transcranial alternating current stimulation: a review of the underlying mechanisms and modulation of cognitive processes,” *Frontiers in human neuroscience*, vol. 7, p. 279, 2013.
- [2] F. Galaz Prieto, A. Rezaei, M. Samavaki, and S. Pursiainen, “L1-norm vs. l2-norm fitting in optimizing focal multi-channel tes stimulation: linear and semidefinite programming vs. weighted least squares,” *Computer Methods and Programs in Biomedicine*, vol. 226, p. 107084, 2022.
- [3] J. P. Dmochowski, A. Datta, M. Bikson, Y. Su, and L. C. Parra, “Optimized multi-electrode stimulation increases focality and intensity at target,” *Journal of neural engineering*, vol. 8, no. 4, p. 046011, 2011.
- [4] J. P. Dmochowski, L. Koessler, A. M. Norcia, M. Bikson, and L. C. Parra, “Optimal use of eeg recordings to target active brain areas with transcranial electrical stimulation,” *Neuroimage*, vol. 157, pp. 69–80, 2017.
- [5] M. Bertero and P. Boccacci, *Introduction to inverse problems in imaging*. CRC press, 2020.
- [6] J. Kaipio and E. Somersalo, *Statistical and computational inverse problems*. Springer Science & Business Media, 2006, vol. 160.
- [7] M. Fernandez-Corazza, S. Turovets, and C. H. Muravchik, “Unification of optimal targeting methods in transcranial electrical stimulation,” *Neuroimage*, vol. 209, p. 116403, 2020.
- [8] S. Wagner, M. Burger, and C. H. Wolters, “An optimization approach for well-targeted transcranial direct current stimulation,” *SIAM Journal on Applied Mathematics*, vol. 76, no. 6, pp. 2154–2174, 2016.
- [9] S. Mehrotra, “On the implementation of a primal-dual interior point method,” *SIAM Journal on optimization*, vol. 2, no. 4, pp. 575–601, 1992.
- [10] S. Boyd and L. Vandenberghe, *Convex Optimization*. Cambridge University Press, 2004. [Online]. Available: <https://books.google.fi/books?id=IUZdAAAAQBAJ>
- [11] Y. Zhang, “User’s guide to lipsol linear-programming interior point solvers v0. 4,” *Optimization Methods and Software*, vol. 11, no. 1-4, pp. 385–396, 1999.
- [12] M. ApS, *The MOSEK optimization toolbox for MATLAB manual. Version 9.1.*, 2019. [Online]. Available: <http://docs.mosek.com/9.1/toolbox/index.html>
- [13] Gurobi Optimization, LLC, “Gurobi Optimizer Reference Manual,” 2022. [Online]. Available: <https://www.gurobi.com>
- [14] R. H. Tütüncü, K.-C. Toh, and M. J. Todd, “Solving semidefinite-quadratic-linear programs using sdpt3,” *Mathematical programming*, vol. 95, no. 2, pp. 189–217, 2003.
- [15] J. F. Sturm, “Using sedumi 1.02, a matlab toolbox for optimization over symmetric cones,” *Optimization methods and software*, vol. 11, no. 1-4, pp. 625–653, 1999.
- [16] J. Sturm, “Central region method. high performance optimization, jbg frenk, c. roos, t. terlaky and s. zhang,” 2000.
- [17] I. Polik, T. Terlaky, and Y. Zinchenko, “Sedumi: a package for conic optimization,” in *IMA workshop on Optimization and Control, Univ. Minnesota, Minneapolis*. Citeseer, 2007.
- [18] M. Grant, S. Boyd, and Y. Ye, “Cvx users’ guide,” in *Tech. Rep. Build*. Cambridge Univ., 2009, p. 711.
- [19] T. Kowalski, J. Silny, and H. Buchner, “Current density threshold for the stimulation of neurons in the motor cortex area,” *Bioelectromagnetics: Journal of the Bioelectromagnetics Society, The Society for Physical Regulation in Biology and Medicine, The European Bioelectromagnetics Association*, vol. 23, no. 6, pp. 421–428, 2002.
- [20] J. Malmivuo and R. Plonsey, “Bioelectromagnetism,” *Medical and Biological Engineering and Computing*, vol. 34, pp. 9–12, 1996.
- [21] I. Dikin, “Iterative solution of problems of linear and quadratic programming,” in *Doklady Akademii Nauk*, vol. 174, no. 4. Russian Academy of Sciences, 1967, pp. 747–748.
- [22] A. V. Fiacco and G. P. McCormick, “The sequential unconstrained minimization technique for nonlinear programming, a primal-dual method,” *Management Science*, vol. 10, no. 2, pp. 360–366, 1964.
- [23] Q. He, A. Rezaei, and S. Pursiainen, “Zeffiro user interface for electromagnetic brain imaging: A gpu accelerated fem tool for forward and inverse computations in matlab,” *Neuroinformatics*, pp. 1–14, 2019.
- [24] A. Rezaei, J. Lahtinen, F. Neugebauer, M. Antonakakis, M. C. Piastra, A. Koulouri, C. H. Wolters, and S. Pursiainen, “Reconstructing subcortical and cortical somatosensory activity via the RAMUS inverse source analysis technique using median nerve SEP data,” *NeuroImage*, vol. 245, p. 118726, 2021.
- [25] T. Miinalainen, A. Rezaei, D. Us, A. Nüßing, C. Engwer, C. H. Wolters, and S. Pursiainen, “A realistic, accurate and fast source modeling approach for the eeg forward problem,” *NeuroImage*, vol. 184, pp. 56–67, 2019.
- [26] S. Pursiainen, F. Lucka, and C. H. Wolters, “Complete electrode model in EEG: relationship and differences to the point electrode model,” *Phys. Med. Biol.*, vol. 57, no. 4, pp. 999–1017, 2012.
- [27] S. Pursiainen, B. Agsten, S. Wagner, and C. H. Wolters, “Advanced boundary electrode modeling for tes and parallel tes/eeg,” *IEEE Transactions on Neural Systems and Rehabilitation Engineering*, vol. 26, no. 1, pp. 37–44, 2017.
- [28] B. Fischl, “Freesurfer,” *Neuroimage*, vol. 62, no. 2, pp. 774–781, 2012.
- [29] M. Dannhauer, B. Lanfer, C. H. Wolters, and T. R. Knösche, “Modeling of the human skull in EEG source analysis,” *Human Brain Mapping*, vol. 32, no. 9, pp. 1383–1399, 2011.
- [30] S. Bayliss, G. A. Constantinides, W. Luk *et al.*, “An fpga implementation of the simplex algorithm,” in *2006 IEEE international conference on field programmable technology*. IEEE, 2006, pp. 49–56.
- [31] F. Gensheimer, S. Ruzika, S. Scholl, and N. Wehn, “A simplex algorithm for lp decoding hardware,” in *2014 IEEE 25th Annual International Symposium on Personal, Indoor, and Mobile Radio Communication (PIMRC)*. IEEE, 2014, pp. 790–794.
- [32] T. Lin, S. Ma, Y. Ye, and S. Zhang, “An admm-based interior-point method for large-scale linear programming,” *Optimization Methods and Software*, vol. 36, no. 2-3, pp. 389–424, 2021.
- [33] D. N. Anderson, B. Osting, J. Vorwerk, A. D. Dorval, and C. R. Butson, “Optimized programming algorithm for cylindrical and directional deep brain stimulation electrodes,” *Journal of neural engineering*, vol. 15, no. 2, p. 026005, 2018.